Far infrared laser magnetic resonance of singlet methylene: Singlet–triplet perturbations, singlet–triplet transitions, and the singlet–triplet splitting[a)]

A. R. W. McKellar, P. R. Bunker, and Trevor J. Sears

Herzberg Institute of Astrophysics, National Research Council of Canada, Ottawa, Canada K1A OR6

K. M. Evenson and R. J. Saykally[b)]

National Bureau of Standards, Boulder, Colorado 80303

S. R. Langhoff

NASA Ames Research Center, Moffett Field, California 94035
(Received 5 August 1983; accepted 22 August 1983)

We have observed and assigned a number of far infrared laser magnetic resonance spectra of CH_2 arising from rotational transitions within the lowest vibrational state of the $\tilde{a}\,^1A_1$ electronic excited state and from transitions between such singlet levels and vibrationally excited levels of the $\tilde{X}\,^3B_1$ electronic ground state. The singlet–singlet transitions are magnetically active, and the singlet–triplet transitions have electric dipole intensity, because of the spin-orbit mixing of singlet levels with vibrationally excited levels of the triplet state. By identifying four pairs of singlet and triplet levels that perturb each other we can accurately position the singlet and triplet state relative to each other and determine the single–triplet energy splitting. We determine that $T_0(\tilde{a}\,^1A_1) = 3165 \pm 20$ cm^{-1} (9.05 ± 0.06 kcal/mol; 0.392 ± 0.003 eV), and $T_e(\tilde{a}\,^1A_1) = 2994 \pm 30$ cm^{-1} (8.56 ± 0.09 kcal/mol; 0.371 ± 0.004 eV). A new *ab initio* calculation of the spin-orbit matrix element between these two states has been of assistance in assigning the levels that perturb each other and has enabled us to calculate the radiative lifetimes of the lowest *ortho* and *para* levels of the $\tilde{a}\,^1A_1$ state to be about 18 s in each case.

I. INTRODUCTION

There is widespread interest in the spectroscopy, dynamics, and relative energies of the two lowest electronic states of methylene CH_2. The ground state is a triplet ($\tilde{X}\,^3B_1$) and the first excited state is a singlet ($\tilde{a}\,^1A_1$). Methylene was first observed spectroscopically by Herzberg,[1] who detected both of these states in absorption and concluded that the triplet state was the ground electronic state. This energy ordering was confirmed by the observation[2] of the ESR spectrum of matrix-isolated triplet CH_2. The structure of the singlet state was determined in the classic work of Herzberg and Johns,[3] but the structure of the triplet ground state has only recently been established in detail[4,5] by means of LMR (laser magnetic resonance) spectroscopy in the far- and mid-infrared regions[6–10] and subsequent microwave[11] and diode laser[12] studies.

The separation in energy of the singlet and triplet states has been the subject of some controversy. Recent *ab initio* calculations[13–25] give values around 3500 ± 300 cm^{-1} (10.0 ± 0.9 kcal/mol or 0.43 ± 0.04 eV) for $T_e(\tilde{a}\,^1A_1)$, and experiments involving kinetics and heats of formation[26–34] give about 3000 ± 300 cm^{-1} (8.5 ± 0.9 kcal/mol; 0.37 ± 0.04 eV) for $T_0(\tilde{a}\,^1A_1)$. However, the most direct experimental determination,[35,36] from the laser photodetachment spectrum of CH_2^-, was interpreted to give a much larger singlet–triplet splitting of 6800 cm^{-1} (19.5 kcal/mol; 0.85 eV). For more extensive discussions of the history of research into the singlet–triplet energy difference in methylene, the reader is referred to the introductions of the recent papers by Lengel and Zare,[32] Hayden *et al.*,[34] Engelking *et al.*,[36] and Saxe *et al.*[23]

In the present paper we report the assignment of a number of far infrared LMR spectra to transitions among rotational levels of the vibrational ground state of the $\tilde{a}\,^1A_1$ state, and to singlet–triplet transitions between levels of the $\tilde{a}\,^1A_1$ and $\tilde{X}\,^3B_1$ states. These singlet–singlet and singlet–triplet transitions give rise to LMR spectra because of perturbations between the $\tilde{a}\,^1A_1$ and $\tilde{X}\,^3B_1$ states. The spin-orbit coupling interaction responsible for the perturbations is studied with the help of *ab initio* calculations, and some singlet and triplet levels that perturb each other are identified using the nonrigid bender Hamiltonian. This leads to a direct determination of the singlet–triplet splitting: $T_0(\tilde{a}\,^1A_1) = 3165 \pm 20$ cm$^-$ (9.05 ± 0.06 kcal/mol; 0.392 ± 0.003 eV; 94.9 ± 0.6 THz), and $T_e(\tilde{a}\,^1A_1) = 2994 \pm 30$ cm^{-1} (8.56 ± 0.09 kcal/mol; 0.371 ± 0.004 eV, 89.8 ± 0.9 THz). These values constitute the most precise and reliable measurement of this quantity. In an accompanying paper[37] a new simulation of the CH_2^- photodetachment spectrum,[36] using the best available potential energy curves and rotation-vibration transition intensities, is shown to be in accord with this value of the singlet–triplet splitting.

The organization of this paper is as follows. In Sec. II, we present the observed LMR spectra, and show

a)Research supported in part by NASA contract W-15,047.
b)Present address: Department of Chemistry, University of California, Berkeley, CA 94720.

 0021-9606/83/235251-14$02.10

how a Zeeman analysis results in unambiguous assignments to certain CH_2 $\tilde{a}\,^1A_1$ state transitions perturbed by triplet state levels with definite N values. In Sec. III, we give the results of new *ab initio* calculations of the spin-orbit interaction between the $\tilde{a}$ and $\tilde{X}$ states as a function of molecular geometry. Section IV draws on the results of the two preceding sections, and uses predictions from the nonrigid bender Hamiltonian,[5] to show that there is a unique positioning of the $\tilde{a}$ singlet state relative to the $\tilde{X}$ triplet state which explains the experimental observations. In Sec. V, we estimate the radiative lifetimes of the lowest *ortho* and *para* rotational levels of the $\tilde{a}\,^1A_1$ state, and in Sec. VI we offer concluding remarks.

II. EXPERIMENTAL RESULTS AND ZEEMAN ANALYSIS

A. Apparatus and chemistry

The spectra reported here were obtained at the NBS Boulder laboratory using the far infrared LMR spectrometer described previously.[7] Methylene radicals were produced in a flow system by discharging a mixture of F_2 and He, and reacting the resulting F atoms with CH_4. A similar fluorine–methane flame has been used[7] to study the rotational spectrum of ground state ($\tilde{X}\,^3B_1$) CH_2, and it also yields LMR spectra of the species C, CH, C_2H, CF, and CH_2F. Compared with ground state CH_2,[7] the spectra reported here exhibited maximum intensity with a "hotter" flame, that is, with relatively more F_2 and CH_4 and a higher total pressure. Typical operating pressures were 200, 10, and 8 Pa (1 Pa = 7.5 mTorr), respectively, for He, F_2, and CH_4.

B. Analysis of the spectra

We have observed and assigned LMR spectra using 11 different far-infrared laser lines. The assignments involve five rotational transitions within the vibrational ground state of $\tilde{a}\,^1A_1$ CH_2 = $7_{25} - 7_{16}$, $7_{16} - 7_{07}$, $8_{27} - 8_{18}$, $9_{45} - 9_{36}$, and $4_{31} - 4_{22}$. The assignments were made, with the help of the approximately known[3] term values for the $\tilde{a}$ state, by performing Zeeman analyses in which the effects of triplet state perturbations were allowed for. Below we detail each analysis in turn.

1. *The $7_{25} \rightarrow 7_{16}$ and $7_{16} \leftarrow 7_{07}$ transitions*

In the course of observing far-infrared LMR spectra of CH_2, a number of "inverted" lines were observed[7,38] which appeared to be due to transitions showing gain, rather than loss, in the LMR spectrometer. These inverted spectra are exemplified by the series illustrated in Fig. 1, which was observed using a laser line at 58.2216 cm^{-1} (171.8 μm). The chemistry used ($F + CH_4$) and the apparent triplet hyperfine structure suggested that the spectrum might be due to CH_2. However, it could not be assigned to $\tilde{X}\,^3B_1$ CH_2 and it exhibited a number of distinctive features not shared with the ordinary[7] triplet LMR spectrum of CH_2:

(1) the phase of each line is inverted, implying gain and thus population inversion,

(2) there is a coincidence of π and σ transitions; i.e., each component of the series appears in parallel (π) and perpendicular (σ) polarization at the same magnetic field, and

(3) the line progression is characteristic of a nearly linear Zeeman effect, in that a plot of line number vs

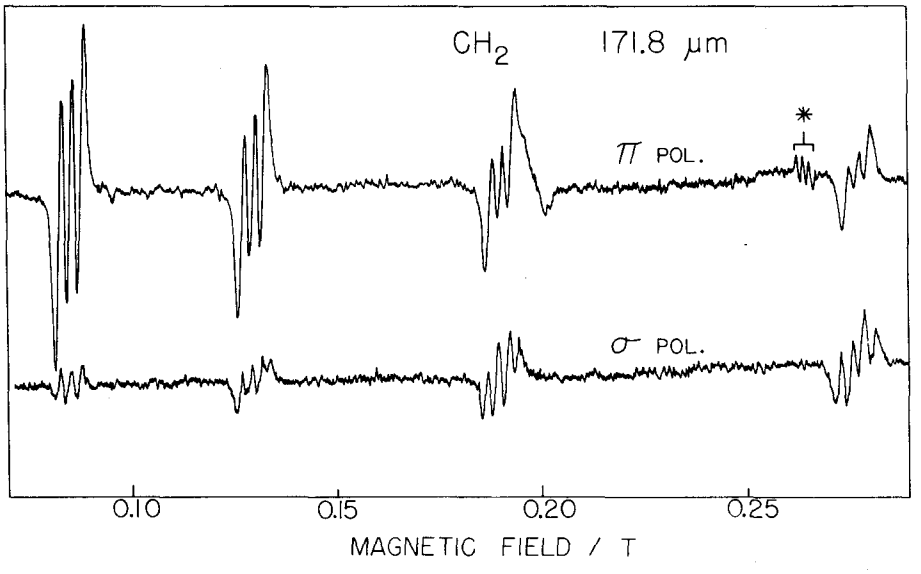

FIG. 1. Laser magnetic resonance spectrum of CH_2 obtained with the 58.2216 cm^{-1} (171.8 μm) laser line of $^{13}CH_3OH$ with the laser radiation polarized parallel (π) and perpendicular (σ) relative to the applied magnetic field. Note the inverted line shape, which indicates gain rather than absorption by this transition (an unrelated triplet with normal line shapes is indicated by an asterisk in the π trace). Note also the coincidence of π and σ components, and the triplet hyperfine structure (the appearance of more than three components in the higher field σ lines is the beginning of a split into $\Delta M_J = +1$ and -1 components which becomes more evident in further members of the series at higher fields).

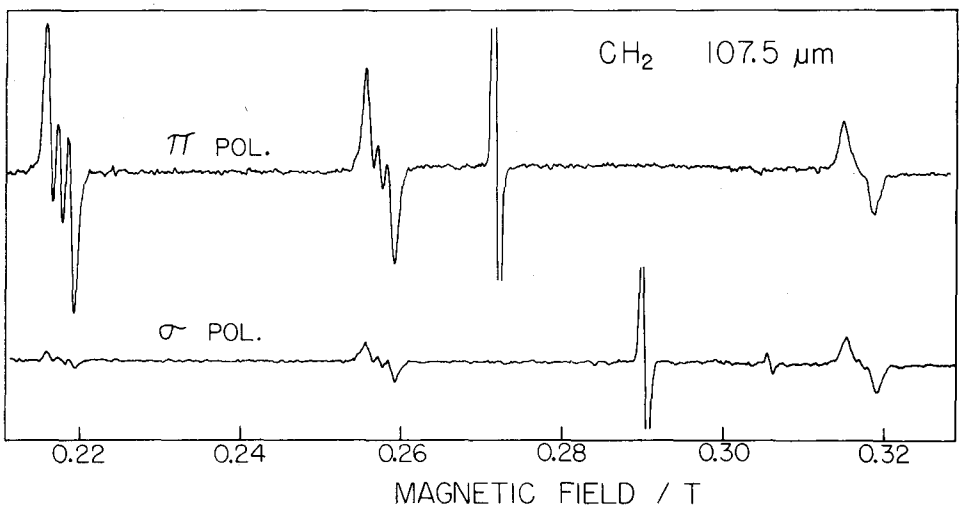

FIG. 2. LMR spectrum of CH_2 obtained with the 92.9906 cm^{-1} (107.5 μm) laser line of CD_3OD. The series of interest here, with lines at 0.2178, 0.2578, and 0.3169 T (see Table I), shows a normal lineshape with triplet hyperfine structure and coincident σ and π features. The strong single lines near 0.27 T in π and 0.29 T in σ, as well as the weak line near 0.305 T in σ, are components of the $2_{12} \leftarrow 1_{01}$ transition in ground state CH_2, (000) $\tilde{X}\,^3B_1$. This transition was extensively observed using a different laser line in Ref. 7.

the reciprocal of the magnetic field yields a straight line.

The characteristics listed above can all be accounted for in terms of singlet–triplet perturbations in CH_2 in the following manner: the lower level of a rotational transition in the $\tilde{a}\,^1A_1$ state is perturbed by a level of the $\tilde{X}\,^3B_1$ state, with the appropriate J value, located a few cm^{-1} away. Many CH_2 molecules are initially produced in the singlet manifold, and the channels for intramolecular relaxation to the ground triplet state are limited. The perturbed singlet level thus loses population, relative to other singlet levels, as molecules "leak" out to the perturbing triplet level. This loss sets up the population inversion that produces the inverted spectrum. The coincidence of the π and σ transitions is a simple consequence of the fact that the perturbed (lower) level possesses all the Zeeman effect while the upper level is virtually diamagnetic. Finally, the linear character of the Zeeman effect results from the perturbed singlet level being separated from the perturbing triplet level, and its associated spin components, by a few cm^{-1} (this point is examined quantitatively below). Some of the observed LMR transitions are from the unperturbed upper singlet level to the perturbing triplet level; if the level mixing is large, this singlet–triplet transition will share the characteristics of the perturbed singlet–singlet transition.

Some other observed characteristics help to identify the 171.8 μm spectrum of Fig. 1. The observed intensities of the components (in π polarization, the intensities decrease with increasing field, and in σ polarization the opposite occurs) suggest that we are observing a Q-branch transition. A $1/B$ plot based on the near linearity of the Zeeman pattern suggests that $J \approx 7$ for the perturbed level. And finally, the triplet hyperfine structure means that *ortho*-CH_2 levels of $\tilde{a}\,^1A_1$ must be involved (those with $K_a + K_c$ = odd number). Thus even without detailed calculation, there are two prime candidates for the 171.8 μm spectrum: the $7_{25} - 7_{16}$ (expected at about 62 cm^{-1})[39] and $7_{43} - 7_{34}$ (about 59 cm^{-1}) transitions in the ground vibrational state of $\tilde{a}\,^1A_1$.

Subsequent experiments resulted in observations of this same inverted transition with two other nearby laser lines at 57.8549 and 58.6248 cm^{-1} which confirmed the $J = 7$ assignment. In addition a different but related inverted spectrum was observed with laser lines at 59.9964 and 60.0128 cm^{-1}. For a quantitative analysis of the spectra, we adopted a model based on the following 4×4 Hamiltonian matrix:

$$H_{11} = E_1 + \Gamma M_J/(N+1)\,, \tag{1}$$

$$H_{22} = E_2 + \Gamma M_J/[N(N+1)]\,, \tag{2}$$

$$H_{33} = E_3 - \Gamma M_J/N\,, \tag{3}$$

$$H_{12} = [\Gamma/(N+1)][N(N+M_J+1)(N-M_J+1)/(2N+1)]^{1/2}\,, \tag{4}$$

$$H_{23} = [\Gamma/N][(N+1)(N+M_J)(N-M_J)/(2N+1)]^{1/2}\,, \tag{5}$$

$$H_{44} = E_S\,, \tag{6}$$

$$H_{14} = W_{SO}\,, \tag{7}$$

where $\Gamma = g_s \mu_B B$, and E_1, E_2, and E_3 are the energies of the F_1, F_2, and F_3 spin components of a triplet state level (with $J = N+1$, N, and $N-1$, respectively). Equations (1)–(5) represent the isotropic approximation to the Zeeman effect for a given $(N_{K_a K_c})$ triplet state level.[7] Here we simply add a singlet level having energy E_S and an interaction matrix element W_{SO} connecting it with one of the triplet components. In Eq. (7), we assume that the singlet level has $J = N+1$ and thus interacts with F_1; an interaction with F_2 or F_3 is similarly modeled by replacing Eq. (7) with $H_{24} = W_{SO}$ or $H_{34} = W_{SO}$. Note that at this stage the singlet level is assumed to have no Zeeman effect of its own, and that the singlet–triplet perturbation (7) is also assumed to be field independent.

By applying Eqs. (1)–(7) to the observed data in a

TABLE I. Observed LMR spectra involving the 7_{16} level of the $\tilde{a}^1A_1$ state of CH_2.

Laser line[a] (cm^{-1})	Assignment[b] $N_{K_aK_c}$	J	M_J	Resonant field (T)	Obs–Calc (cm^{-1})
57.854 90	$7_{25} \rightarrow t$	$7 \rightarrow 7$	7	0.8341	+0.0004
			6	0.9316	+0.0001
			5	1.0506	+0.0001
58.221 58	$7_{25} \rightarrow t$	$7 \rightarrow 7$	7	0.1425	+0.0000
			6	0.1649	+0.0001
			5	0.1952	+0.0001
			4	0.2381	+0.0000
			3	0.3030	+0.0000
			2	0.4080	−0.0000
			1	0.5895	−0.0001
			0	0.9005	−0.0001
			−1	1.3524	−0.0003
58.624 77	$7_{25} \rightarrow t$	$7 \rightarrow 7$	−7	0.6981	−0.0003
			−6	0.8524	+0.0013[c]
			−5	1.1602	−0.0006
59.996 41	$7_{25} \rightarrow t$	$7 \rightarrow 6$	−5	1.1430	+0.0003
			−4	1.1680	−0.0002
			−3	1.2200	+0.0000
			−2	1.2935	+0.0000
			−1	1.4006	−0.0002
			0	1.5521	−0.0002
			1	1.7723	−0.0000
60.012 83	$7_{25} \rightarrow t$	$7 \rightarrow 6$	−5	1.1240	−0.0002
			−4	1.1480	−0.0004
			−3	1.1962	−0.0002
			−2	1.2700	+0.0003
			−1	1.3735	+0.0002
			0	1.5198	+0.0001
			1	1.7320	+0.0000
65.064 40	$7_{25} \rightarrow s$	$7 \rightarrow 7$	−7	0.7711	−0.0002
			−6	0.8696	+0.0020[c]
			−5	0.0059	−0.0002
			−4	1.1750	−0.0002
			−3	1.3967	−0.0006
			−2	1.6829	−0.0002
86.338 45	$s \leftarrow 7_{07}$	$7 \leftarrow 7$	−7	0.7378	+0.0001
			−6	0.8380	+0.0001
			−5	0.9655	−0.0000
			−4	1.1314	+0.0000
			−3	1.3487	−0.0001
			−2	1.6354	−0.0003
92.990 65	$t \leftarrow 7_{07}$	$7 \leftarrow 7$	−7	0.2178	−0.0000
			−6	0.2578	+0.0000
			−5	0.3169	−0.0000
			−4	0.4174	+0.0001
			−3	0.6532	+0.0001

[a]The eight far-infrared laser lines used here are generated in the following gases: CH_2DOH, $^{13}CH_3OH$, CH_3OH, CH_2F_2, CH_2F_2, $^{13}CD_3OH$, $^{13}CH_3OH$, CD_3OD.

[b]In order to save space, we list here only the parallel polarization (π) portion of the spectrum ($\Delta M_J = 0$). Where only σ transitions were observed, the average of the two components is given. In the $N_{K_aK_c}$ column, 7_{25} and 7_{07} are unperturbed levels of the $\tilde{a}^1A_1$ state, "s" stands for the perturbed 7_{16} level of the $\tilde{a}^1A_1$ state, and "t" stands for the perturbing triplet level with $N=6$, which in Sec. IV is assigned as $(030)6_{15}$ of $\tilde{X}\,^3B_1$. Right arrows ($\rightarrow$) denote "inverted" (gain) transitions and left arrows ($\leftarrow$) denote "regular" (loss) transitions.

[c]Note that there is some evidence here for a very small perturbation of the $M_J = -6$ component of the 7_{25} level.

nonlinear least-squares fitting program, we determined that the perturbed lower state of the transition could be well represented by a triplet level with $N=6$ interacting with a singlet level with $J=7$. The spectra near 58 cm^{-1} were found to involve the perturbed F_1 triplet level with $J=7$, those at 60 cm^{-1} involved the F_2 triplet level with $J=6$, and the true singlet–singlet transition was predicted to occur at 64.6 cm^{-1}. This latter transition was subsequently observed as an inverted series using a laser line at 65.0644 cm^{-1}. From the analysis, the unperturbed position of the $\tilde{a}\,^1A_1$ rotational transition could be estimated as 61.8 cm^{-1}, thus favoring its assignment as $7_{25} - 7_{16}$ (see above). This rotational assignment was then confirmed by observing the $7_{16} - 7_{07}$ transition using laser lines at 86.3384 and 92.9906 cm^{-1}, and part of the latter spectrum is shown in Fig. 2. These $7_{16} - 7_{07}$ spectra appeared as regular (noninverted) series, just as expected since the perturbed 7_{16} level is the upper state of the transition.

Spectra observed using eight different laser lines could now be simultaneously analyzed using a model involving the same Zeeman-active levels. The collected data are listed in Table I together with their assignments. Parameters resulting from the least-squares fit are given in Table II, and the good quality of the fit may be seen in the Obs-Calc column of Table I. A small Zeeman effect was observed for the "unperturbed" 7_{25} level of $\tilde{a}\,^1A_1$, which was clearly mainfested as a doubling of the observed $7_{25} - 7_{16}$ lines in σ polarization into $\Delta M_J = -1$ and $+1$ components at high field. This was accounted for by assuming a simple linear Zeeman effect:

$$E_s(J_{K_aK_c};\, B) = E_s(J_{K_aK_c};\, 0) + g_{\rm eff}(J_{K_aK_c})\mu_B B M_J/(J+1)\,, \tag{8}$$

and the resulting value for $g_{\rm eff}(7_{25})$ is given in Table II. No such splittings were resolved for the 7_{07} level. How-

TABLE II. Parameters obtained from a least-squares fit to the data of Table I.

Parameter	Value[a]	Unit
$E_s(7_{16})$	0[b]	cm^{-1}
E_1	+0.4849(89)	cm^{-1}
E_2	+0.9106(56)	cm^{-1}
E_3	+0.6706(48)	cm^{-1}
W_{SO}	3.201 28(12)	cm^{-1}
$E_s(7_{25})$	61.7462(49)	cm^{-1}
$E_s(7_{25}) - E_s(7_{07})$	151.3926(2)	cm^{-1}
$g_{\rm eff}(7_{16})$	+0.019(4)	...
$g_{\rm eff}(7_{25})$	+0.0188(8)[c]	...
$g_{\rm eff}(7_{07})$	0[d]	...

[a]Uncertainties in parentheses are one standard error from the least-squares fit.

[b]The zero of energy is arbitrarily chosen here as the (unperturbed) position of the singlet 7_{16} level.

[c]Effective g value required to fit the small Zeeman splittings observed for the singlet 7_{25} level.

[d]No Zeeman splittings were resolved for the singlet 7_{07} level.

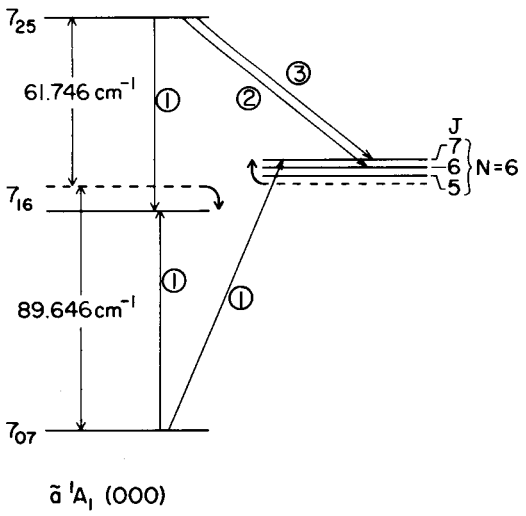

FIG. 3. Illustration of the energy levels involved in the $7_{25} \rightarrow 7_{16}$ and $7_{16} \leftarrow 7_{07}$ transitions considered in Sec. II B 1 (not drawn to scale). The perturbing triplet level with $N=6$ is drawn on the right, and the dashed lines indicate the positions of the levels before perturbation. The numbers in circles give the number of different laser lines used to observe each transition. A more detailed view of the center part of this figure is given in Fig. 4.

ever, it seems reasonable to allow the perturbed 7_{16} level also to possess a small first order Zeeman effect, which may arise through the rotational Zeeman effect (see below). Thus Eq. (6) was replaced by Eq. (8) in the final fit, and the resulting g value for 7_{16} is given in Table II; it is remarkably close to that determined for 7_{25}.

The relative positions of the triplet spin components E_1, E_2, and E_3 determined here are an aid in identifying the perturbing triplet level (see Sec. IV below). The deperturbed singlet energy intervals $7_{25} - 7_{16} = 61.75$ cm^{-1} and $7_{25} - 7_{07} = 151.39$ cm^{-1} (Table II) compare favorably with the values[39] from our semirigid bender (62.39 and 152.59 cm^{-1}) and conventional (61.66 and 151.33 cm^{-1}) fits to the data of Herzberg and Johns.[3] Illustrations of the energy levels analyzed here are shown in Figs. 3 and 4, and the precise assignment of the $N=6$ perturbing triplet level is considered in Sec. IV.

2. *The $8_{27} \rightarrow 8_{18}$ transition*

Another spectrum consisting of a series of inverted components was observed using a laser line at 102.6029 cm^{-1} (97.5 μm). Like the 171.8 μm spectrum, the components were apparently hyperfine triplets, the π and σ transitions coincided, and the relative intensities suggested a Q-branch transition. Unfortunately, it was not possible to obtain any further observations of this transition, mainly because of the relatively low density of available laser lines above 100 cm^{-1}. Analysis indicated that the series could be well fitted as a singlet Q-branch transition with $J=8$ having its lower level perturbed by a triplet state level with $N=9$. A consideration of the possible $\tilde{a}\ ^1A_1$ state transitions strongly suggested the assignment as $8_{27} \rightarrow 8_{18}$.

The observed resonant fields and assignments for the 97.5 μm spectrum are listed in Table III. As in the case of the 171.8 μm spectrum, this new spectrum is actually a singlet–triplet transition, occurring between the relatively unperturbed $\tilde{a}\ ^1A_1$ 8_{27} level and the perturbing triplet level with $N=9$ and $J=8$. The parameters resulting from a fit to the measurements of Table III are given in Table IV. Since data from only one laser line are available, the parameters here are much less well determined than those in Table II. In particular, there is very high correlation between the interaction matrix element W_{SO} and the unperturbed separation of the singlet and triplet levels, and we chose to fix W_{SO} in the fit. The analysis yields a value of 105.2 cm^{-1} for the deperturbed $\tilde{a}\ ^1A_1$ $8_{27} - 8_{18}$ transition frequency, which may be compared with estimates of 106.8 and 106.6 cm^{-1} from our semirigid bender and conventional fits to the $\tilde{a}$ state.[39] The perturbed singlet–singlet transition should occur around 106.6 cm^{-1}, but unfortunately there were no laser lines available in this region.

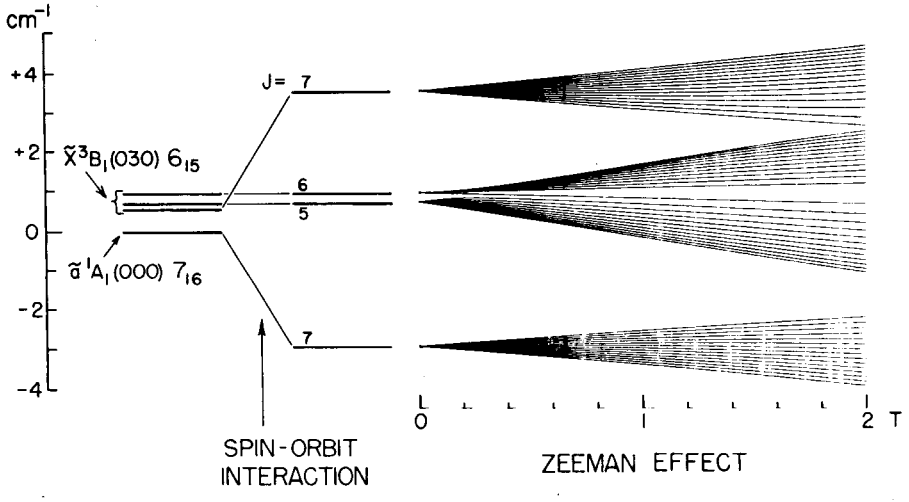

FIG. 4. Illustration of the interaction between the $\tilde{a}\ ^1A_1(000)7_{16}$ level of CH_2 and the perturbing triplet state level with $N=6$. The (arbitrary) zero of the energy scale is consistent with Table II. The nearly linear Zeeman effect of the two $J=7$ levels at low fields is evident here.

TABLE III. LMR spectra of the $8_{27} \leftarrow 8_{18}$ transition in $\tilde{a}^1A_1$ CH_2, observed with the 96.5 μm laser line of CH_3OH (103.692 901 cm^{-1}).

Assignment[a]			Resonant field (T)	Obs–Calc (cm^{-1})
$N_{K_a K_c}$	J	M_J		
$8_{27} \leftarrow t$	$8 \leftarrow 8$	$-8 \leftarrow -8$	0.0994	+0.0001
		$-7 \leftarrow -7$	0.1115	−0.0001
		$-6 \leftarrow -6$	0.1275	−0.0001
		$-5 \leftarrow -5$	0.1485	+0.0000
		$-4 \leftarrow -4$	0.1765	+0.0001
		$-3 \leftarrow -3$	0.2145	+0.0000
		$-2 \leftarrow -2$	0.2675	−0.0001
		$-1 \leftarrow -1$	0.3435	+0.0000
		$-1 \leftarrow 0$	0.4445	−0.0000
		$0 \leftarrow 1$	0.5745	+0.0000
		$2 \leftarrow 1$	0.5777	−0.0000
		$2 \leftarrow 2$	0.7265	+0.0001
		$1 \leftarrow 2$	0.7245	+0.0000
		$3 \leftarrow 2$	0.7280	−0.0000
		$3 \leftarrow 3$	0.8840	−0.0000
		$2 \leftarrow 3$	0.8825	+0.0000
		$4 \leftarrow 3$	0.8860	+0.0000
		$4 \leftarrow 4$	1.0380	−0.0000
		$3 \leftarrow 4$	1.0362	−0.0001
		$5 \leftarrow 4$	1.0395	−0.0001
		$5 \leftarrow 5$	1.1795	+0.0000
		$4 \leftarrow 5$	1.1780	+0.0000
		$6 \leftarrow 5$	1.1810	+0.0001
		$6 \leftarrow 6$	1.3030	−0.0001
		$5 \leftarrow 6$	1.3020	+0.0001
		$7 \leftarrow 6$	1.3045	+0.0001
		$7 \leftarrow 7$	1.4065	−0.0001
		$8 \leftarrow 8$	1.4897	+0.0000

[a]8_{27} is the unperturbed level of the $\tilde{a}^1A_1$ state, and t stands for the perturbing triplet level with $N = 9$, which in Sec. IV is assigned as (020) 9_{37} of $\tilde{X}^3B_1$.

3. The $9_{45} \leftarrow 9_{36}$ transition

Two series of normal (noninverted) lines were observed using a laser line at 49.1073 cm^{-1} (203.6 μm) and subsequently also observed using a nearby laser line at 49.3913 cm^{-1} (202.5 μm). One of these series consisted of barely resolved hyperfine triplets arranged in a distinctive pattern which was quite unlike those observed at 171.8 and 97.5 μm. It was found that this series could be very well represented as a singlet state Q-branch transition with $J = 9$ whose upper level was perturbed by a triplet state level with $N = 9$. The perturbation by an F_2 level (rather than F_1 or F_3 as in the two previous examples) was responsible for the different appearance of the series, since the Zeeman effect is very different for F_2 levels due to an additional factor of N in the denominator of Eq. (2). A consideration of the possible singlet state rotational transitions indicated the assignment of this series to be $9_{45} \leftarrow 9_{36}$.

The observed resonant fields and assignments for this transition are listed in Table V, and the parameters resulting from a least-squares fit are given in Table VI. The two laser lines used to observe this transition are quite close together, and it turns out that the parameters in the fit are not too well determined because of the high

TABLE IV. Parameters obtained from a least-squares fit to the data of Table III.

Parameter	Value[a]	Unit
$E_s(8_{18})$	0[b]	cm^{-1}
E_1	0.08(24)	cm^{-1}
E_2	0.41(23)	cm^{-1}
E_3	0.10(44)	cm^{-1}
W_{SO}	1.47[c]	cm^{-1}
$E_s(8_{27}) - E_s(8_{18})$	105.17(23)	cm^{-1}
$g_{eff}(8_{18})$	+0.023(11)	...
$g_{eff}(8_{27})$	+0.0122(11)	...

[a]Uncertainties in parentheses are one standard error from the least-squares fit.
[b]The zero of energy is arbitrarily chosen here as the (unperturbed) position of the singlet 8_{18} level.
[c]Because of the limited available data, we chose to fix W_{SO} at a value which is consistent both with this analysis and that in Sec. IV below.

TABLE V. LMR spectra of the $9_{45} \leftarrow 9_{36}$ transition in $\tilde{a}^1A_1$ CH_2.

Laser line[a] (cm^{-1})	Assignment[b]			Resonant field (T)	Obs–Calc (cm^{-1})
	$N_{K_a K_c}$	J	M_J		
49.107 282	$t \leftarrow 9_{36}$	$9 \leftarrow 9$	$-1 \leftarrow -1$	0.9682	+0.0001
			$0 \leftarrow 0$	0.9692	+0.0000
			$-2 \leftarrow -2$	0.9729	+0.0000
			$1 \leftarrow 1$	0.9762	+0.0001
			$-3 \leftarrow -3$	0.9839	−0.0001
			$2 \leftarrow 2$	0.9891	−0.0000
			$-4 \leftarrow -4$	1.0016	−0.0002
			$3 \leftarrow 3$	1.0089	−0.0001
			$-5 \leftarrow -5$	1.0280	−0.0000
			$4 \leftarrow 4$	1.0371	+0.0001
			$-6 \leftarrow -6$	1.0643	−0.0000
			$5 \leftarrow 5$	1.0749	−0.0001
			$-7 \leftarrow -7$	1.1140	−0.0001
			$6 \leftarrow 6$	1.1259	+0.0000
			$-8 \leftarrow -8$	1.1831	+0.0001
			$7 \leftarrow 7$	1.1948	+0.0002
			$-9 \leftarrow -9$	1.2808	−0.0002
			$8 \leftarrow 8$	1.2894	−0.0003
49.391 266	$t \leftarrow 9_{36}$	$9 \leftarrow 9$	$2 \leftarrow 2$	0.5775	+0.0000
			$-4 \leftarrow -4$	0.5803	+0.0000
			$3 \leftarrow 3$	0.5955	−0.0000
			$-5 \leftarrow -5$	0.6007	−0.0001
			$4 \leftarrow 4$	0.6212	+0.0000
			$-6 \leftarrow -6$	0.6315	+0.0001
			$5 \leftarrow 5$	0.6568	−0.0002
			$-7 \leftarrow -7$	0.6763	−0.0001
			$6 \leftarrow 6$	0.7081	+0.0001
			$-8 \leftarrow -8$	0.7462	+0.0001
			$7 \leftarrow 7$	0.7830	−0.0001
			$-9 \leftarrow -9$	0.8653	+0.0001
			$8 \leftarrow 8$	0.9032	+0.0000

[a]The 49.107 and 49.391 cm^{-1} laser lines are generated in $^{13}CH_3OH$ and CH_2F_2, respectively.
[b]In order to save space, we list here only the π components ($\Delta M_J = 0$) of the spectrum. Measurements with a common M'_J have been averaged to obtain these field values. In the $N_{K_a K_c}$ column, 9_{36} is the unperturbed $\tilde{a}^1A_1$ state lower level, and t stands for the perturbing triplet state level with $N = 9$, which in Sec. IV is assigned as (020)9_{46} of $\tilde{X}^3B_1$.

TABLE VI. Parameters obtained from a least-squares fit to the data of Table V.

Parameter	Value[a]	Unit
$E_s(9_{45})$	0[b]	cm^{-1}
E_1	−1.9770(5)	cm^{-1}
E_2	−1.928(72)	cm^{-1}
E_3	−1.9513(4)	cm^{-1}
W_{SO}	1.58(15)	cm^{-1}
$E_s(9_{45})-E_s(9_{36})$	52.41(29)	cm^{-1}
$g_{eff}(9_{45})$	+0.0311(19)	•••
$g_{eff}(9_{36})$	+0.0210(4)	•••

[a]Uncertainties in parentheses are one standard error from the least-squares fit. There are large correlations among the parameters in the fit, and the true uncertainties are probably larger than those listed here.

[b]The zero of energy is arbitrarily chosen here as the (unperturbed) position of the singlet 9_{45} level.

TABLE VII. LMR spectra of the $4_{31} \leftarrow 4_{22}$ transition in $\tilde{a}^1A_1$ CH_2.

Laser line[a] (cm^{-1})	Assignment[b] $N_{K_a K_c}$	J	M_J	Resonant field (T)	Obs−Calc (cm^{-1})
49.107 282	$t \leftarrow 4_{22}$	4←4	4←4	1.1695	+0.0001
			4←3	1.1674	−0.0000
			3←3	1.2139	−0.0002
			3←2	1.2115	−0.0001
			3←4	1.2161	−0.0001
			2←2	1.2617	+0.0003
			2←1	1.2597	+0.0000
			2←3	1.2644	+0.0000
			1←0	1.3129	−0.0000
			1←2	1.3177	+0.0000
			0←−1	1.3714	+0.0002
			0←1	1.3763	+0.0003
			−1←−2	1.4374	−0.0004
			−1←0	1.4426	−0.0005
			−2←−3	1.5096	+0.0002
			−2←−1	1.5151	+0.0001
49.391 266	$t \leftarrow 4_{22}$	4←4	4←4	1.4987	+0.0001
			4←3	1.4961	−0.0000
			3←3	1.5386	+0.0002
			3←2	1.5361	−0.0001
			3←4	1.5418	−0.0001
			2←2	1.5831	+0.0001
			2←1	1.5804	−0.0001
			2←3	1.5861	−0.0000
			1←1	1.6326	−0.0000
			1←0	1.6295	+0.0001
			1←2	1.6353	+0.0002
			0←−1	1.6845	+0.0001
			0←1	1.6907	+0.0000
			−1←−2	1.7463	−0.0001
			−1←0	1.7525	−0.0001

[a]The laser lines are the same as in Table V.

[b]In the $N_{K_a K_c}$ column, 4_{22} is the unperturbed $\tilde{a}^1A_1$ state lower level, and t stands for the perturbing triplet state level with $N=3$, which in Sec. IV is assigned as $(030)3_{12}$ of $\tilde{X}^3B_1$.

TABLE VIII. Parameters obtained from a least-squares fit to the data of Table VII.

Parameter	Value[a]	Unit
$E_s(4_{31})$	0[b]	cm^{-1}
E_1	2.01(16)	cm^{-1}
E_2	2.09(17)	cm^{-1}
E_3	1.87(17)	cm^{-1}
W_{SO}	0.968(47)	cm^{-1}
$E_s(4_{31})-E_s(4_{22})$	45.74(17)	cm^{-1}
$g_{eff}(4_{31})$	0[c]	•••
$g_{eff}(4_{22})$	0.0175(3)	•••

[a]Uncertainties in parentheses are one standard error from the least-squares fit.

[b]The zero of energy is arbitrarily chosen here as the (unperturbed) position of the singlet 4_{31} level.

[c]This parameter was not well determined in the fit, and hence was set equal to zero.

correlation between W_{SO} and $E_2 - E_S$. The analysis yields 52.4 cm^{-1} for the deperturbed $\tilde{a}^1A_1$ $9_{45} - 9_{36}$ transition frequency; this is close to the estimate of 54.1 cm^{-1} from both of our singlet state fits.[39]

4. *The $4_{31} \leftarrow 4_{22}$ transition*

The other series observed on the 203.6 and 202.5 μm laser lines had a simpler pattern than that of the $9_{45} \leftarrow 9_{36}$ transition, apparently consisted of hyperfine singlets, and, like the other series treated here, had an intensity pattern indicating it was due to a Q-branch transition. We assigned it to the $\tilde{a}^1A_1$ $4_{31} - 4_{22}$ transition with the upper level (4_{31}) perturbed from above by a triplet state level with $N=3$. The observed resonant fields and assignments for this series are listed in Table VII and the parameters determined from a least-squares fit are given in Table VIII. As in the two previous transitions there are large correlations in the fit, and the parameters are not very well determined. The analysis yields 45.7 cm^{-1} for the deperturbed $\tilde{a}^1A_1$ $4_{31} - 4_{22}$ transition frequency, which may be compared with values of 45.5 and 45.7 cm^{-1} from our semirigid bender and conventional fits to the singlet state.[39]

III. *AB INITIO* SPIN-ORBIT MATRIX ELEMENTS

We have calculated the spin-orbit coupling matrix element between the $\tilde{X}^3B_1$ and $\tilde{a}^1A_1$ electronic states of CH_2 using the microscopic spin-orbit Hamiltonian[40,41]

$$H_{SO} = \frac{e^2\hbar}{2m^2c^2}\sum_{iA}\frac{Z_A}{r_{iA}^3}(\mathbf{r}_{iA}\times\mathbf{p}_i)\cdot\mathbf{s}_i + \sum_{i\neq j}(\nabla_i r_{ij}^{-1}\times\mathbf{p}_i)\cdot(\mathbf{s}_i+2\mathbf{s}_j), \tag{9}$$

where Z_A is the charge on nucleus A, and $\mathbf{p}_i$ and $\mathbf{s}_i$ are the momenta and spin of electron i. Calculations were carried out at bond angles of 90°, 112°, and 135.1° with the CH bond length fixed at 1.096 Å. The sensitivity of the $\langle\tilde{X}^3B_1|H_{SO}|\tilde{a}^1A_1\rangle$ matrix elements to basis set was examined by carrying out calculations with a double-zeta plus polarization basis[42,43] (9*s*5*p*1*d*/5*s*1*p*) contracted to [4*s*2*p*1*d*/3*s*1*p*] and an extended (near

TABLE IX. Spin-orbit coupling matrix elements between the $^3B_1$ and $^1A_1$ states of CH_2.

Basis set[a]	Energy selection criterion (μh)[b]		CI energies (a.u.)		$^1A_1$ coefficients[c]		$\langle ^3B_1\, m_S=0 \mid H_{SO} \mid ^1A_1\, m_S=0\rangle$[d] ($cm^{-1}$)
	$^3B_1$	$^1A_1$	$^3B_1$	$^1A_1$	a	b	
(A) 90°							
DZP	10	10	−39.0182	−39.0266	0.954	−0.163	11.715
Extended	10	10	−39.0442	−39.0530	0.955	−0.144	13.068
(B) 112°							
DZP	10	10	−39.0482	−39.0279	0.948	−0.204	11.664
Extended	10	10	−39.0737	−39.0538	0.950	−0.179	13.182
(C) 135.1°							
DZP	100	100	−39.0416	−38.9986	0.942	−0.233	11.639
DZP	10	10	−39.0530	−39.0117	0.927	−0.287	10.457
DZP	10	1	−39.0530	−39.0134	0.923	−0.298	10.216
Extended	100	100	−39.0431	−39.0000	0.945	−0.219	12.543
Extended	10	10	−39.0787	−38.0381	0.932	−0.262	11.840

[a]DZP and extended refer to the [4*s*2*p*1*d*/3*s*1*p*] and [7*s*4*p*2*d*/3*s*2*p*] contracted Cartesian Gaussian basis sets.
[b]All single excitations were kept. Doubles were selected by Rayleigh–Schrödinger perturbation theory and kept in the wave function if more than the designated threshold. The reference space for the $^3B_1$ state was $1a_1^2\,2a_1^2\,1b_2^2\,3a_1^1\,1b_1^1$ and for $^1A_1$ state was the two configurations $1a_1^2\,2a_1^2\,3a_1^2\,1b_2^2$ and $1a_1^2\,2a_1^2\,1b_1^2\,1b_2^2$.
[c]Coefficients of the $1a_1^2\,2a_1^2\,3a_1^2\,1b_2^2$ and $1a_1^2\,2a_1^2\,1b_1^2\,1b_2^2$ configurations in the CI wave functions.
[d]Note that the matrix elements in Table II of Ref. 45 are a factor of $\sqrt{2}$ smaller because they are defined between wave functions with $m_S = S$.

Hartree–Fock quality) basis,[44] (13*s*7*p*2*d*/6*s*2*p*) contracted to [7*s*4*p*2*d*/3*s*2*p*]. Since the matrix element is sensitive to electron correlation effects,[45] it was calculated with increasingly larger configuration-interaction (CI) wave functions. The results for the $\langle \tilde{X}\,^3B_1,\ m_S=0 \mid H_{SO} \mid \tilde{a}\,^1A_1,\ m_S=0\rangle$ matrix element are summarized in Table IX.

Although the $\tilde{X}\,^3B_1$ state is well described by the single configuration $\mid 1a_1^2 2a_1^2 1b_2^2 3a_1^1 1b_1^1\rangle$, an equivalent description of the $\tilde{a}\,^1A_1$ state requires the linear combination of the two configurations $a\mid 1a_1^2 2a_1^2 1b_2^2 3a_1^2\rangle + b\mid 1a_1^2 2a_1^2 1b_2^2 1b_1^2\rangle$. The spin-orbit coupling matrix element is substantially reduced by CI, because the coefficient b is negative and both the $\tilde{a}\,^1A_1$ configurations have similar matrix elements with the dominant configuration of the $\tilde{X}\,^3B_1$ state. When double excitations are generated from both $\tilde{a}\,^1A_1$ configurations and selected (using the criterion of their energy correction) the coefficient b becomes larger as the selection threshold is decreased. Hence the matrix element decreases with increasing CI, and in the singles plus doubles limit would probably be several tenths of 1 cm^{-1} less than the values obtained using the 10 μh ($\simeq 2$ cm^{-1}) selection criterion. In contrast the spin-orbit coupling matrix elements increase as the basis set in enlarged. However, the extended basis is nearly complete so it is unlikely that any further significant changes would arise from the addition of *f* functions or further saturation of the *s*, *p*, and *d* spaces. The extended basis set CI results (at 10 μh) are probably within 5% of the correct values.

The $\langle \tilde{X}\,^3B_1 \mid H_{SO} \mid \tilde{a}\,^1A_1\rangle$ matrix element decreases with increasing bond angle, eventually becoming zero for the linear configuration. In large part the change in the matrix element with bond angle can also be understood in terms of the magnitude of the coefficient b. As the bond angle increases b becomes larger until at 180° $b = -a = -2^{1/2}$. The extended basis 10 μh CI results at 90°, 112°, and 135.1° were fitted to a polynomial in the angle ρ ($\rho = \pi - \alpha$) to give (in cm^{-1})

$$H_{SO}^{Xa}(\rho) = \langle \tilde{X}\,^3B_1 \mid H_{SO} \mid \tilde{a}\,^1A_1\rangle = 5.54 + 11.54\rho - 4.29\rho^2 \ . \tag{10}$$

The singlet–triplet bending overlaps are negligible near linearity where this expression fails. The matrix element is not expected to depend markedly on the bond lengths and this dependence was not calculated.

The matrix elements of the function given in Eq. (10) between various vibrational states of the $\tilde{a}\,^1A_1$ and $\tilde{X}\,^3B_1$ electronic states are given in Table X. The bending wave functions used in this calculation are those ob-

TABLE X. *Ab initio* vibronic matrix elements of the spin-orbit coupling operator H_{SO}.[a]

$\tilde{a}\,^1A_1$ (v_1, v_2, v_3)	$\tilde{X}\,^3B_1$ (v_1', v_2', v_3')	$\langle \tilde{a};\ v_1 v_2 v_3 \mid H_{SO} \mid \tilde{X};\ v_1' v_2' v_3'\rangle$ (cm^{-1})
(0 0 0)	(0 0 0)	2.3
(0 0 0)	(1 0 0)	0.6
(0 0 0)	(0 0 1)	0.6
(0 0 0)	(0 1 0)	−3.6
(0 0 0)	(0 2 0)	4.5
(0 0 0)	(0 3 0)	−5.5
(0 0 0)	(0 4 0)	5.7
(0 0 0)	(0 5 0)	−4.9
(0 1 0)	(1 1 0)	−1.3
(0 1 0)	(1 1 1)	−1.3
(0 1 0)	(0 4 0)	−3.6

[a]Using the expression given in Eq. (10).

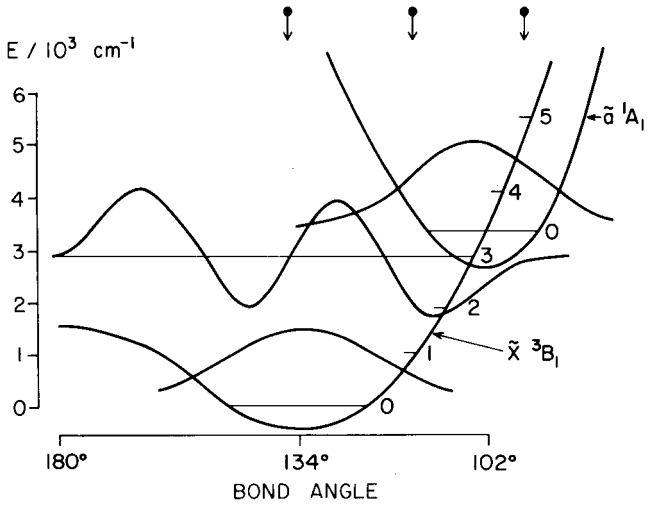

FIG. 5. The bending potential curves of the $\tilde{a}\,^1A_1$ and $\tilde{X}\,^3B_1$ states of CH_2 determined by semirigid bender fits. Wave functions for $v_2 = 0$ of the $\tilde{a}$ state and $v_2 = 3$ and 0 of the $\tilde{X}$ state are shown; these illustrate why the spin-orbit matrix element for $\tilde{a}(000)$ with $\tilde{X}(030)$ is larger than that for $\tilde{a}(000)$ with $\tilde{X}(000)$. The arrows at the top of the figure indicate the three angles for which the *ab initio* calculations of H_{SO} were carried out.

tained using the semirigid bender Hamiltonian for each state with $K_a = 0$ (see Ref. 37). The stretching wave functions are obtained by representing each stretching potential as a Morse oscillator with $\omega_e = 3000$ cm^{-1}, dissociation energy $D_e = 36\,000$ cm^{-1}, $R_e(\tilde{a}\,^1A_1) = 1.124$ Å, and $R_e(\tilde{X}\,^3B_1) = 1.084$ Å. The R_e values are the values of R at the minima of the bending potential curves in the semirigid bender calculations. The stretching potential functions lead to small off-diagonal Franck–Condon factors; the overlaps $\langle v' | v'' \rangle$ for either the ν_1 or ν_3 states are 0.97 if $v' = v'' = 0$, 0.91 if $v' = v'' = 1$, and 0.25 if $v' = 0$ (for the singlet state) and $v'' = 1$ (for the triplet state).

The singlet and triplet bending potential curves and three of the bending wave functions are shown in Fig. 5. From this figure we can appreciate why the $\tilde{X}$-state level $v_2 = 3$ has a significantly larger spin-orbit matrix element with the $\tilde{a}$-state level $v_2 = 0$ than the $\tilde{X}$-state level $v_2 = 0$. The (1, 0, 0) and (0, 0, 1) levels of the triplet state have rather small spin-orbit coupling matrix elements with the (0, 0, 0) level of the singlet state because of the small overlaps of these stretching wave functions.

IV. ASSIGNMENT OF PERTURBING TRIPLET LEVELS

The four rotational levels 4_{31}, 7_{16}, 8_{18}, and 9_{45} of the ground vibrational state of $\tilde{a}\,^1A_1$ CH_2 have each been observed to be perturbed by a nearby level of the $\tilde{X}\,^3B_1$ state, as we show in Sec. II above. In this section, we assign the perturbing triplet levels using a knowledge of the predicted rotation-vibration levels of the triplet state,[5] and of the restrictions imposed by symmetry on the values of N, K_a, K_c for the perturbing levels. The *ab initio* values of the spin-orbit coupling matrix elements from Sec. III provide useful assistance, and confirmation, in making the assignments.

Using experimentally determined[6–12] energy level separations for $^{12}CH_2$, $^{13}CH_2$, and CD_2, the geometry and potential function of the $\tilde{X}\,^3B_1$ state has been determined using the nonrigid bender Hamiltonian.[5] The input data do not involve levels with $v_2 \geq 2$, $K_a \geq 3$, $\Delta v_1 \neq 0$, or $v_3 \neq 0$, but the positions of such levels can still be calculated using the nonrigid bender program. The predicted triplet state energy levels were examined in order to find a set of four levels with the correct relative spacing, N values, and symmetries to perturb the four singlet state levels. We originally thought that the $\tilde{X}\,^3B_1$ excited stretching states were prime candidates for the perturbing levels, especially in view of the observation of FIR LMR transitions within the (100) state.[7] However, as indicated in Table X, such states have much smaller spin-orbit coupling matrix elements with the $\tilde{a}\,^1A_1$ (000) state than do the $\tilde{X}\,^3B_1$ bending states (020), (030), and (040) which occur in the same energy region. This limitation restricted the search to levels with $v_2 < 6$ and $v_3 = v_1 = 0$, and only one set of four such triplet state energy levels was found for which the predicted separations match the perturbed singlet level separations to better than 20 cm^{-1}. These four triplet levels and the perturbed singlet levels are shown in Fig. 6. Also indicated in Fig. 6 are the experimental and theoretical values of the interaction matrix elements W_{SO} for each pair of levels (the calculation of these theoretical values is considered in the following paragraph). Of the experimental matrix elements, that for the singlet 7_{16} level $W_{SO} = 3.201$ cm^{-1}, is by far the most reliable. It agrees rather well with the *ab initio* value of 3.0 cm^{-1}, and this agreement provides strong supporting evidence for our assignment of the perturbing levels.

In Sec. III and Table X we considered the calculation of the vibronic part of the spin-orbit interaction between singlet and triplet state levels. Here we give some further details, add the effects of molecular rotation,

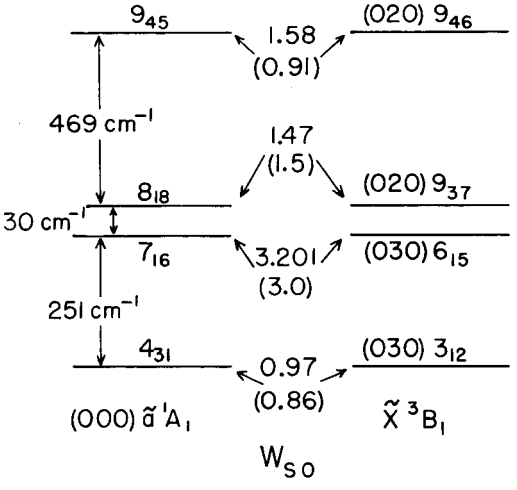

FIG. 6. Perturbed energy levels in the $\tilde{a}\,^1A_1$ state of CH_2 together with the levels of the $\tilde{X}\,^3B_1$ state responsible for the perturbations. The numbers in the center of the figure are values (in cm^{-1}) of the spin-orbit interaction matrix elements responsible for the perturbations; theoretical values are in parentheses.

and arrive at theoretical values for W_{SO}. Making the Born–Oppenheimer and semirigid bender approximations, we can write the vibronic eigenfunctions of the singlet ($\tilde{a}$) and triplet ($\tilde{X}$) states as the following product of electronic ψ_e, rotation-bending ψ_{rb}, and stretching ψ_s states:

$$\psi^a_{rve} = \psi^a_e \psi^a_{rb} \psi^a_s \tag{11}$$

and

$$\psi^X_{rve} = \psi^X_e \psi^X_{rb} \psi^X_s \, . \tag{12}$$

The rovibronic matrix element of the spin-orbit coupling operator H_{SO} of Eq. (9) is

$$W_{SO} = \langle \psi^X_{rve} | \, H_{SO} \, | \psi^a_{rve} \rangle = \langle \psi^X_s | \, \psi^a_s \rangle \, \langle \psi^X_{rb} | \, H^{Xa}_{SO}(\rho) \, | \psi^a_{rb} \rangle \, , \tag{13}$$

where $H^{Xa}_{SO}(\rho)$ is given in Eq. (10). The stretching overlap elements $\langle \psi^X_s | \psi^a_s \rangle$ are calculated numerically using the assumed Morse function potential curves described in Sec. III to give the following values for $\langle v^X_1 v^X_3 | \, v^a_1 v^a_3 \rangle = \langle v^X_1 | \, v^a_1 \rangle \langle v^X_3 | \, v^a_3 \rangle$:

$$\langle 00 | \, 00 \rangle = 0.97 \times 0.97 = 0.94 \tag{14}$$

and

$$\langle 01 | \, 00 \rangle = \langle 10 | \, 00 \rangle = 0.97 \times 0.25 = 0.24 \, . \tag{15}$$

The semirigid bender functions ψ^i_{rb} can each be written

$$\psi^i_{rb} = \sum_{k, v_2} c^J_i(k, \, v_2) \, | Jk \rangle \, \phi^i_{k, v_2}(\rho) \, , \tag{16}$$

where $| J, k \rangle$ is a symmetric top rotational wave function (for the triplet state, we use $| N, k \rangle$), $\phi^i_{k, v_2}(\rho)$ is a bending wave function which depends on k because of the centrifugal distortion effect of k rotation on the bending potential function [see Eq. (11) of Bunker and Landsberg[46]], and the $c^J_i(k, \, v_2)$ are expansion coefficients determined in the diagonalization of the semirigid bender Hamiltonian. The rotation-bending matrix elements of $H^{Xa}_{SO}(\rho)$ are obtained as

$$\langle \psi^X_{rb} | \, H^{Xa}_{SO}(\rho) \, | \psi^a_{rb} \rangle = \sum_{k, k', v_2, v'_2} c^N_X(k, \, v_2)^* \, c^J_a(k, \, v'_2) \times \langle Nk | \, Jk' \rangle \langle \phi^X_{k, v_2}(\rho) | \, H^{Xa}_{SO}(\rho) | \, \phi^a_{k', v'_2}(\rho) \rangle \, . \tag{17}$$

The rotational factors $\langle Nk | \, Jk' \rangle$ were obtained from Table I of Stevens and Brand.[47]

The resulting calculated *ab initio* matrix elements of the $\tilde{a}\,^1A_1$ (000) 7_{16} level with possible perturbing $\tilde{X}\,^3B_1$ levels with $N = 6$ and possible values of K_a and K_c are shown in Table XI. On this basis alone, the assignment shown in Fig. 6 of the perturbing level as (030) 6_{15} is the most likely. The uncertainties in the other three experimental spin-orbit matrix elements are considerably greater than that for 7_{16}, but they too are generally consistent with the calculated values.

The first excited stretching states (100) and (001) of $\tilde{X}\,^3B_1$ almost certainly lie in the appropriate energy range to perturb the $\tilde{a}\,^1A_1$ (000) state, and they may indeed be involved in such perturbations. However, as we have seen, the magnitudes of the four perturbations identified in Sec. II are too large to be interpreted as being due to stretching levels.

A comparison of calculated triplet level spin splittings with those determined experimentally for the perturbing levels (Table II, IV, VI, and VIII) provides a further check on our assignments. In order to calculate the spin splittings, we first estimate a set of spin–spin and spin-rotation parameters for the $\tilde{X}\,^3B_1$ (020) and (030) states, based on the known[7,8] parameters for (000) and (010). For the (030) 6_{15} level, we thus obtain splittings of $E_2 - E_1 = +0.370$ cm^{-1} and $E_3 - E_1 = +0.002$ cm^{-1}. But these splittings will then be perturbed by surrounding singlet state levels in addition to the main perturbed level [$\tilde{a}\,^1A_1$ (000) 7_{16}] that we are explicitly considering. When this effect is allowed for, the calculated splittings change to $E_2 - E_1 = +0.462$ cm^{-1} and $E_3 - E_1 = +0.207$ cm^{-1}, which agree remarkably well with the experimental values of $+0.426$ and $+0.186$ cm^{-1} (Table II). This test is especially effective in disriminating against such levels as $\tilde{X}\,^3B_1$ (030) 6_{33} as the level perturbing $\tilde{a}\,^1A_1$ 7_{16}. Calculated spin splittings also agree well with the observed values for the other assignments in Fig. 6, with the exception of the $\tilde{X}\,^3B_1$ (020) 9_{46} level. This latter case also exhibits the greatest discrepancy between observed and calculated values of W_{SO}, and we feel that there may be a nearby triplet level with $N = 9$ from an excited stretching state which contributes an additional perturbation to the $\tilde{a}\,^1A_1$ 9_{45} level.

TABLE XI. Values of *ab initio* coupling matrix elements W_{SO} for the $\tilde{a}\,^1A_1$ (000)7_{16} level with various $\tilde{X}\,^3B_1$ $(v_1 v_2 v_3)$ $6_{K_a K_c}$ levels.

v_1	v_2	v_3	K_a	K_c	W_{SO} (cm^{-1})
1	0	0	any	any	< 0.3[a]
0	0	1	any	any	< 0.3[a]
0	any	0	5	1	< 0.4[a]
0	any	0	3	3	< 2.4[a]
0	0	0	1	5	-1.3
0	1	0	1	5	2.1
0	2	0	1	5	-2.8
0	3	0	1	5	3.0
0	4	0	1	5	-2.9
0	5	0	1	5	2.3
0	6	0	1	5	-1.7

[a]Absolute value of W_{SO} is less than this value.

Having identified the triplet levels that perturb the singlet state levels, we now wish to determine their energies above the $\tilde{X}\,^3B_1$ (000) 0_{00} and $\tilde{a}\,^1A^1$ (000) 0_{00} rovibronic ground levels in order to obtain the singlet–triplet separation $T_0(\tilde{a}\,^1A_1)$. The singlet energy levels are fairly well determined by the work of Herzberg and Johns.[3,39] For the triplet state, using the nonrigid bender energy levels from Ref. 5 we obtain, for example, the unperturbed energy of the (030) 6_{15} level above $\tilde{X}\,^3B_1$ (000) 0_{00} as 3703.4 cm^{-1}. For a slight refinement, we can do a new nonrigid bender fit to the triplet state by adding the three deperturbed separations of the triplet state levels discussed here (with weights of 0.1) to the 61 levels used in Ref. 5 (with weights of 1), and then obtain a value of 3697.3 cm^{-1} for this energy. Taking averaged singlet state energy levels from our two fits,[39] and triplet energies from this new nonrigid bender fit, we obtain a value for the singlet–triplet splitting of $T_0(\tilde{a}\,^1A_1) = 3165 \pm 20$ cm^{-1}. The quoted uncertainty of

± 20 cm^{-1} represents our estimate of the possible systematic and model errors involved in calculating the extrapolated triplet state rotation-bending levels. Extended observations of CH_2 $\tilde{X}\,^3B_1$ state spectra should enable this uncertainty to be reduced in the future (e.g., observation of the (020) state by means of the $v_2 = 2 \leftarrow 0$ overtone or $2 \leftarrow 1$ hot bands in the infrared).

The calculated bending zero point energies are 670 cm^{-1} in the $\tilde{a}\,^1A_1$ state and 499 cm^{-1} in $\tilde{X}\,^3B_1$. Assuming that the stretching zero-point energies are very similar for the two states, we thus obtain a value of $T_e(\tilde{a}\,^1A_1) = 2994 \pm 30$ cm^{-1}.

V. DIPOLE TRANSITION STRENGTHS AND THE RADIATIVE LIFETIME OF THE SINGLET STATE

Two of us[48] have calculated *ab initio* the electric dipole moment of CH_2 at several nuclear geometries both in the $\tilde{X}\,^3B_1$ and $\tilde{a}\,^1A_1$ electronic states, and have determined rovibrational transition moments within each state. Disappointingly we found that the transition moments for the ν_1 and ν_3 fundamental stretching bands of $\tilde{X}$ state CH_2 are very small (0.003 D) and thus that these bands will be very hard to detect. In confirmation of previous results we found that the dipole moment in the $\tilde{a}\,^1A_1$ state is relatively large (1.7 D)—three times larger than that in the $\tilde{X}\,^3B_1$ state. These results mean that singlet–triplet transitions such as reported in the present paper, which involve a pure rotation transition moment in the singlet state, will be the singlet–triplet transitions with the largest transition moment; singlet–triplet transition originating in the ground state of the triplet state will have a very small transition moment.

The lowest *para* ($I=0$) and *ortho* ($I=1$) rotational levels of the singlet state are the $J_{K_aK_c} = 0_{00}$ and 1_{01} levels, respectively, of the (000) vibrational state. Radiative decay from these levels, into levels of the triplet state can occur as a result of the spin-orbit interaction between the triplet and singlet states. Knowing the rotation-vibration transition moments for the triplet state, and the spin-orbit coupling function for the singlet and triplet states, we can calculate the transition probabilities for transitions from these levels to any triplet state level, and hence determine their radiative lifetimes.

The lifetime of a level $|i\rangle$ of the $\tilde{a}$ state is given by

$$\tau_i = 1/\sum_j A_{ij} \ , \tag{18}$$

where

$$A_{ij}/\mathrm{s}^{-1} = 3.14\times10^{-7}(\omega_{ij}/\mathrm{cm}^{-1})^3 \left|\langle i|(\mu/\mathrm{D})|j\rangle\right|^2 \ . \tag{19}$$

The $|j\rangle$ are levels in the $\tilde{X}$ state, below the level $|i\rangle$, to which dipole transitions can occur, $\omega_{ij} = E_i - E_j$, and μ is the dipole moment function. If we let $|a_i\rangle$ be the zeroth order (pure singlet) rovibronic wave function for the state $|i\rangle$, and $|X_j\rangle$ be the zeroth order (pure triplet) rovibronic wave function for the state $|j\rangle$, then

$$\langle i|\mu|j\rangle = \sum_k \frac{\langle a_i|H_{SO}|X_k\rangle\langle X_k|\mu|X_j\rangle}{\omega_{ik}} \ , \tag{20}$$

where $|X_k\rangle$ are "intermediate" zeroth order triplet state levels; the mixing of $|X_k\rangle$ with $|a_i\rangle$ by the spin-orbit operator H_{SO} makes the forbidden singlet–triplet transition $|i\rangle \leftarrow |j\rangle$ possible. We use the *ab initio* values of H_{SO} and μ to calculate the matrix elements occurring in Eq. (20). The triplet state energies are taken from the nonrigid bender Hamiltonian fit reported at the end of Sec. VI, and the energies of the 0_{00} and 1_{01} levels of the $\tilde{a}$ state are taken as 3165 and 3183 cm^{-1} above the 0_{00} level of (000) $\tilde{X}\,^3B_1$, also from the results of Sec. IV. We present the results of the calculation of the lifetime of the 0_{00} level in some detail but just outline the calculation for the 1_{01} level.

TABLE XII. Spin-orbit matrix elements and energies of triplet state levels mixed with the $\tilde{a}\,^1A_1$ (000)0_{00} level.

$\|X_K\rangle$	$W_{SO} = \langle\tilde{a}(000)0_{00}\|H_{SO}\|X_K\rangle$ (cm^{-1})	E_K (cm^{-1})
(040)1_{01}	5.67	4022
(030)1_{01}	−5.52	2834
(020)1_{01}	4.50	1844
(010)1_{01}	−3.57	978
(000)1_{01}	2.28	16
(100)1_{01}	0.58	2965[a]
(001)1_{11}	−0.43	3153[a]

[a]There is considerable uncertainty in the energies of these excited stretching state levels (see the text).

The 0_{00} level of the vibrational ground state of the $\tilde{a}$ state has symmetry A_1, and it can be mixed by H_{SO} to the $J=0$ fine structure component of any 1_{01} level of a v_3 even state, or 1_{11} level of a v_3 odd state, of the $\tilde{X}$ state. These matrix elements of H_{SO} are calculated using Eqs. (10) and (17). For all the relevant $\tilde{X}$ state levels (called X_k) the matrix elements and energies are given in Table XII.

The final level $|X_j\rangle$ of the transitions can be any $\tilde{X}$ state level below the 0_{00} level of the $\tilde{a}$ state with $J=0$ or 1 and with symmetry A_2. Considering only transitions with $\Delta N = \Delta J$ the following levels are important: The 1_{10} ($J=0$) and 2_{12} ($J=1$) levels of the (000), (100), (010), and (020) vibrational states, and the 2_{02} ($J=1$) level of the (001) state. Using the *ab initio* dipole moment values,[48] the transition moment matrix elements can be calculated and these are given in Table XIII (the rotational factor of $(3/2)^{1/2}$ is included in these matrix elements).

Combining the results of Tables XII and XIII, and using Eq. (20), we obtain the transition moments given in Table VII. The A_{ij} values are calculated using Eq. (11) and these are also given in Table VII. These results when used in Eq. (18) lead to a lifetime for the 0_{00} level of the $\tilde{a}$ state of 18 s.

This lifetime is subject to one significant uncertainty, and this is the position of the (001)1_{11} level of the triplet state which we do not know very precisely. If this level is in *exact* resonance with the 0_{00} level of the $\tilde{a}$ (000) state then the transition moment $\langle\tilde{a}(000)0_{00}|\mu|\tilde{X}(000)2_{12}$ or $1_{10}\rangle$ would be increased to 0.003 D, the A_{ij} value for transitions to (000)2_{12} and 1_{10} would be increased to

TABLE XIII. Rovibrational transition moments within the $\tilde{X}\,^3B_1$ state of CH_2 (in D).

	1_{10} or 2_{12}				2_{02}
$\|X_K\rangle$	(000)	(010)	(020)	(100)	(001)
$(040)1_{01}$	−0.0007	−0.0057	0.0367	•••	•••
$(030)1_{01}$	−0.0047	0.0222	0.3718	•••	•••
$(020)1_{01}$	0.0142	0.2519	−0.5435	•••	•••
$(010)1_{01}$	0.1171	−0.6249	0.0343	•••	•••
$(000)1_{01}$	−0.7055	0.0509	0.0133	−0.0036	•••
$(100)1_{01}$	−0.0036	•••	•••	−0.7055	•••
$(001)1_{11}$	•••	•••	•••	•••	−0.0030

TABLE XIV. Transition moments and radiative decay rates from the $\tilde{a}\,^1A_1$ $(000)0_{00}$ level of CH_2.

$\|X_j\rangle$	E_j (cm^{-1})	$\langle\tilde{a}(000)0_{00}\|\mu\|X_j\rangle$ (D)	A_{ij} (s^{-1})
$(001)2_{02}$	3127[a]	−0.025	7×10^{-6}
$(100)2_{12}$	3058[a]	−0.0017	1×10^{-6}
$(100)1_{10}$	3029[a]		2×10^{-6}
$(020)2_{12}$	2230	−0.0086	1.86×10^{-2}
$(020)1_{10}$	2202		2.04×10^{-2}
$(010)2_{12}$	1162	0.0016	6.4×10^{-3}
$(010)1_{10}$	1133		6.7×10^{-3}
$(000)2_{12}$	108	−0.0004	1.4×10^{-3}
$(000)1_{10}$	79		1.5×10^{-3}

[a]There is considerable uncertainty in the energies of these excited stretching state levels.

TABLE XV. Transition moments and radiative decay rates from the $\tilde{a}\,^1A_1$ $(000)1_{01}$ level of CH_2.

$\|X_j\rangle$	E_j (cm^{-1})	$\langle\tilde{a}(000)1_{01}\|\mu\|X_j\rangle$ (D)	A_{ij} (s^{-1})
$(020)1_{11}$	2200	−0.000 43	6×10^{-5}
$(020)2_{11}$	2234	−0.008 9	2.16×10^{-2}
$(020)3_{13}$	2275	−0.008 0	1.53×10^{-2}
$(010)1_{11}$	1132	0.000 00	•••
$(010)2_{11}$	1165	0.001 63	6.9×10^{-3}
$(010)3_{13}$	1206	0.001 46	5.2×10^{-3}
$(000)1_{11}$	78	0.000 11	1.1×10^{-4}
$(000)2_{11}$	112	−0.000 75	5.2×10^{-3}
$(000)3_{13}$	153	−0.000 36	1.1×10^{-3}

0.080 and 0.083 s^{-1}, respectively, and the lifetime of the $\tilde{a}\,(000)0_{00}$ level would be reduced to 4.5 s.

The lifetime of the 1_{01} level of the $\tilde{a}\,(000)$ state is calculated in a similar manner, and the transition moments, and A_{ij} values, are given in Table XIV. The lifetime is also 18 s but if the level $(001)1_{10}$ of the triplet state is in exact resonance with this state its lifetime is reduced to 4.5 s. The radiative lifetime of the $\tilde{a}$ state of CH_2 has also been calculated by Phillips and Davidson[50] who obtain a value of 40 to 100 s. However, these authors completely ignore the effects of rotation and vibration.

VI. DISCUSSION AND SUMMARY

The relatively high strength of our observed far infrared LMR spectra corresponding to rotational transitions in the excited $\tilde{a}\,^1A_1$ state of CH_2 is not too surprising in view of the molecule's large dipole moment in this state. The calculated[48] dipole moment values are 1.74 D for the $\tilde{a}$ state and 0.58 D for the $\tilde{X}$ state, and thus the singlet state spectra studied here inherently nine times stronger than those[7] of the ground triplet state. A further reason for increased (and highly variable) spectral intensities is the decidedly nonequilibrium rotational population distribution in the $\tilde{a}$ state, as indicated by the observation of inverted spectra.

We have observed some spectra similar to those in Sec. II that we have not been able to assign. For example, using the 86.338 45 cm^{-1} (115.8 μm) laser line of $^{13}CH_3OH$, a series of inverted singlets was observed in the 0.1 to 0.6 T field range with an intensity pattern characteristic of a P or R (rather than Q) transition. In view of the possibility of perturbed transitions within excited vibrational levels of the $\tilde{a}\,^1A_1$ state, it is not surprising that there should be spectra not assignable to the ground vibrational state. One spectrum, apparently due to CH_2, has remained a puzzle ever since the first observations[38] of the methylene LMR spectrum. It is observed using the 117.210 cm^{-1} (85.3 μm) laser line of $^{13}CH_3OH$, and consists of a very short and simple series of regular hyperfine triplets at low magnetic field (0.01 to 0.03 T). We suggest here a tentative assignment of this spectrum to the $3_{30}-2_{21}$ transition within the (010) excited bending state[3] of $\tilde{a}\,^1A_1$. The observed regular (uninverted) line shape suggests that the upper level (3_{30}) is perturbed by a triplet state level, and the most likely perturbing levels are $\tilde{X}\,^3B_1$ (040) 3_{13} or 4_{13}. Further observations with laser lines in the 85 μm region will be required to confirm this assignment.

Almost all the singlet levels we have observed exhibit a residual Zeeman effect which can be characterized by an effective g factor of +0.015 to +0.030, where g_{eff} is defined in Eq. (8). The situation is summarized in Table XVI, and it should be noted that certain values (those for "unperturbed" levels 9_{36}, 8_{27}, 7_{25}, 7_{07}, and 4_{22}) are well determined directly from the experiment, whereas others (for the perturbed levels 9_{45}, 8_{18}, and 7_{16}) depend somewhat on the details of our analysis. We believe that these g factors are a reflection of a large rotational Zeeman effect in the $\tilde{a}\,^1A_1$ state, caused by mixing with the $\tilde{b}\,^1B_1$ state. These two singlet states form a Renner pair, and correlate with a Δ state in the linear limit. The rotational Zeeman effect can be estimated using an expression[51] of the form

$$g_r^a = 4g_L A\left|\langle\tilde{a}\left|L_a\right|\tilde{b}\rangle\right|^2/(E_{\tilde{a}}-E_{\tilde{b}})\,, \tag{21}$$

where $g_L=1$ (in terms of μ_B), L_a is the orbital angular momentum operator ($\Lambda=2$ for a Δ state), and A is the rotational constant. This formula leads to an approximate value of $g_r^a=-0.024$, and the relation between this rotational g factor and our effective value as defined in Eq. (8) is

$$g_{eff} = -g_r^a K_{eff}^2/J\,, \tag{22}$$

where K_{eff} is the expectation value of J_a for the particular $J_{K_aK_c}$ level, and the minus sign arises simply be-

TABLE XVI. Observed and calculated values of g_{eff} for $\tilde{a}^1A_1$ state levels of CH_2.[a]

$N_{K_aK_c}$	g_{eff}(observed)[b]	g_{eff}(calculated)
9_{45}	+0.0311(19)[c]	+0.0217
9_{36}	+0.0210(4)	+0.0174
8_{27}	+0.0122(11)	+0.0178
8_{18}	+0.023(11)[c]	+0.0064
7_{25}	+0.0188(8)	+0.0152
7_{16}	+0.019(4)[c]	+0.0152
7_{07}	0	+0.0063
4_{31}	Not determined	+0.0515
4_{22}	+0.0175(3)	+0.0198

[a] g_{eff} is defined in Eq. (8). The calculated g factors were determined from the electronic rotational Zeeman effect as described in the text.

[b] From Tables II, IV, VI, and VIII. The uncertainties in parentheses are one standard error from the least-squares fits.

[c] These values derived from perturbed levels are less reliable than the rest.

cause of the conventional definition of rotational g factors. Table XVI lists the calculated values of g_{eff} that result from a value of $g_r^a = -0.024$, and it can be seen that there is reasonable agreement with our observed values. There will be additional contributions to the rotational Zeeman effect not included in Eq. (21), and furthermore there will be contributions to the Zeeman effect of $\tilde{a}^1A_1$ levels due to mixing with $\tilde{X}^3B_1$ levels other than those explicitly considered in Sec. II. Thus we do not expect the agreement between observed and calculated g factors to be any better than that shown in Table XVI.

Of the perturbed singlet state levels of CH_2 that we have assigned here, only 4_{31} and 7_{16} are listed as observed levels in Table 7 of Herzberg and Johns.[3] In view of the large perturbation that 7_{16} suffers, its assignment in Ref. 3 is not reliable,[52] however, the position of the 4_{31} level is of interest, since it definitely seems to be perturbed in the results of Herzberg and Johns,[3] as was also noted by Duxbury.[53] Specifically, the observed[3] asymmetry splitting between 4_{31} and 4_{32} is 0.99 cm^{-1}, whereas the calculated values are 1.35, 1.39, and 1.34 cm^{-1} from Ref. 3, and from our two singlet state fits.[39] From Table VIII, we determine that 4_{31} is shifted downwards by 0.39 cm^{-1}, a value that agrees extremely well in direction and magnitude with that implied by the experimental results of Herzberg and Johns.[3]

In summary, we have assigned a number of observed far-infrared LMR spectra to pure rotational transitions within the $\tilde{a}^1A_1$ state of CH_2 and to $\tilde{a}-\tilde{X}$ singlet–triplet transitions. In each transition, a singlet level is perturbed by a nearby level of the $\tilde{X}^3B_1$ state, and the Zeeman effect borrowed in the perturbation allows the LMR observation. Transitions are observed from the unperturbed singlet levels both to the perturbed singlet levels and to the perturbing triplet levels. The energy separations, N values, and symmetries of the perturbing triplet levels leads us to a unique assignment involving the excited bending states (020) and (030) of the $\tilde{X}^3B_1$ state. This assignment is confirmed by a comparison of observed and calculated spin-orbit interaction matrix elements and triplet spin splittings. Our values of $T_0(\tilde{a}^1A_1) = 3165 \pm 20$ cm^{-1} and $T_e(\tilde{a}^1A_1) = 2994 \pm 30$ cm^{-1} are in good agreement with most other recent determinations, but they are about an order of magnitude more precise than any previous determination. Further infrared spectroscopy on the $\tilde{X}^3B_1$ state of CH_2 may enable the (020) and (030) states to be directly observed, and thus reduce the uncertainty in the singlet–triplet splitting.

ACKNOWLEDGMENTS

We are grateful to P. Jensen and M. Bush for help with some of the programming, and are pleased to acknowledge helpful discussions and correspondence with J. T. Hougen, J. M. Brown, H. Petek, C. B. Moore, J. W. C. Johns, and G. Duxbury.

[1] G. Herzberg and J. Shoosmith, Nature (London) **183**, 1801 (1959); G. Herzberg, Proc. R. Soc. London Ser. A **262**, 291 (1961).
[2] R. A. Bernheim, H. W. Bernard, P. S. Wang, L. S. Wood, and P. S. Skell, J. Chem. Phys. **53**, 1280 (1970); **54**, 3223 (1970); E. Wasserman, W. A. Yager, and V. J. Kuck, Chem. Phys. Lett. **7**, 409 (1970); E. Wasserman, R. S. Hutton, V. J. Kuck, and W. A. Yager, J. Chem. Phys. **55**, 2593 (1971).
[3] G. Herzberg and J. W. C. Johns, Proc. R. Soc. London Ser. A **295**, 107 (1966).
[4] P. Jensen, P. R. Bunker, and A. Hoy, J. Chem. Phys. **77**, 5370 (1982).
[5] P. R. Bunker and P. Jensen, J. Chem. Phys. **79**, 1224 (1983).
[6] T. J. Sears, P. R. Bunker, and A. R. W. McKellar, J. Chem. Phys. **75**, 4731 (1981).
[7] T. J. Sears, P. R. Bunker, A. R. W. McKellar, K. M. Evenson, D. A. Jennings, and J. M. Brown, J. Chem. Phys. **77**, 5348 (1982).
[8] T. J. Sears, P. R. Bunker, and A. R. W. McKellar, J. Chem. Phys. **77**, 5363 (1982).
[9] A. R. W. McKellar and T. J. Sears, Can. J. Phys. **61**, 480 (1983).
[10] P. R. Bunker, T. J. Sears, A. R. W. McKellar, K. M. Evenson, and F. J. Lovas, J. Chem. Phys. **79**, 1211 (1983).
[11] F. J. Lovas, R. D. Suenram, and K. M. Evenson, Astrophys. J. Lett. **267**, L131 (1983).
[12] A. R. W. McKellar, C. Yamada, and E. Hirota, J. Chem. Phys. **79**, 1220 (1983).
[13] C. F. Bender, H. F. Schaefer III, D. R. Franceschetti, and L. C. Allen, J. Am. Chem. Soc. **94**, 6888 (1972); D. R. McLaughlin, C. F. Bender, and H. F. Schaefer III, Theor. Chim. Acta **25**, 352 (1972).
[14] P. J. Hay, W. J. Hunt, and W. A. Goddard III, Chem. Phys. Lett. **13**, 30 (1972).
[15] V. Staemmler, Theor. Chim. Acta **31**, 49 (1973); **35**, 309 (1974).
[16] J. F. Harrison, Acc. Chem. Res. **7**, 378 (1974).
[17] A. H. Pakiari and N. C. Handy, Theor. Chim. Acta **40**, 17 (1974).
[18] M. J. S. Dewar, R. C. Haddon, W.-K. Li, W. Thiel, and P. K. Weiner, J. Am. Chem. Soc. **97**, 4540 (1975).
[19] J. H. Meadows and H. F. Schaefer III, J. Am. Chem. Soc. **98**, 4383 (1976).
[20] L. B. Harding and W. A. Goddard III, J. Chem. Phys. **67**,

1777 (1977); Chem. Phys. Lett. **55**, 217 (1978).
[21]C. W. Bauschlichter and S. Shavitt, J. Am. Chem. Soc. **100**, 739 (1978).
[22]S.-K. Shih, S. D. Peyerimhoff, R. J. Buenker, and M. Peric, Chem. Phys. Lett. **55**, 206 (1978).
[23]P. Saxe, H. F. Schaefer III, and N. C. Handy, J. Phys. Chem. **85**, 745 (1981).
[24]P. R. Taylor, J. Chem. Phys. **74**, 1256 (1981).
[25]H.-J. Werner and E.-A. Reinsch, J. Chem. Phys. **76**, 3144 (1982).
[26]H. M. Frey and G. J. Kennedy, J. Chem. Soc. Chem. Commun. **1975**, 233 (1975); J. Chem. Soc. Faraday Trans. 1 **73**, 164 (1977).
[27]W. L. Hase and P. M. Kelly, J. Chem. Phys. **66**, 5093 (1977).
[28]F. Lahmani, J. Phys. Chem. **80**, 2623 (1976).
[29]K. E. McCulloh and V. H. Dibeler, J. Chem. Phys. **64**, 4445 (1976).
[30]D. Feldman, K. Meier, H. Zacharias, and K. H. Welge, Chem. Phys. Lett. **59**, 171 (1978).
[31]D. L. Monts, T. G. Dietz, M. A. Duncan, and R. E. Smalley, Chem. Phys. **45**, 133 (1980).
[32]R. K. Lengel and R. N. Zare, J. Am. Chem. Soc. **100**, 7495 (1978).
[33]J. W. Simons and R. Curry, Chem. Phys. Lett. **38**, 171 (1976).
[34]C. C. Hayden, D. M. Neumark, K. Shobatake, R. K. Sparks, and Y. T. Lee, J. Chem. Phys. **76**, 3607 (1982).
[35]P. F. Zittel, G. B. Ellison, S. V. O'Neil, E. Herbst, W. C. Lineberger, and W. P. Reinhardt, J. Am. Chem. Soc. **98**, 3731 (1976).
[36]P. C. Engelking, R. R. Corderman, J. J. Wendolowski, G. B. Ellison, S. V. O'Neil, and W. C. Lineberger, J. Chem. Phys. **74**, 5460 (1981).
[37]T. J. Sears and P. R. Bunker, J. Chem. Phys. **79**, 5265 (1983).
[38]K. M. Evenson, R. J. Saykally, and J. T. Hougen, Paper TF-5, 34th Symposium on Molecular Spectroscopy, Columbus, Ohio, 1979.
[39]In order to obtain good estimates of the energies of the rotational levels of the $\tilde{a}^1A_1$ state of CH_2, we first prepared a set of all reliable ground state combination differences from the spectra of Herzberg and Johns (Ref. 3). These were then fitted using two different approaches: a conventional nonrigid asymmetric rotor Hamiltonian, and the semirigid bender Hamiltonian. The data set and semirigid bender fit are described in Ref. 37. The conventional fit was made by varying the three rotational and three diagonal quartic centrifugal distortion parameters. The two off-diagonal quartic parameters and the sextic parameter H_K were fixed at values estimated from those of the H_2O and NH_2 molecules, which are structurally very similar to $\tilde{a}^1A_1$ CH_2. The two sets of singlet CH_2 energy levels agreed very well, and the largest discrepancy for a level relevant to this work was 1.6 cm^{-1}.
[40]H. A. Bethe and E. E. Salpeter, *Quantum Mechanics of One- and Two-Electron Atoms* (Springer, Berlin, 1957).
[41]S. R. Langhoff and C. W. Kern, in *Methods of Electronic Structure Theory*, edited by H. F. Schaefer III (Plenum, New York, 1977).
[42]S. Huzinaga, J. Chem. Phys. **42**, 1293 (1965).
[43]T. H. Dunning, J. Chem. Phys. **53**, 2823 (1970).
[44]F. B. Van Duijneveldt, Research Report RJ945, I.B.M. San Jose, California, 1971.
[45]S. R. Langhoff, J. Chem. Phys. **61**, 3881 (1974).
[46]P. R. Bunker and B. M. Landsberg, J. Mol. Spectrosc. **67**, 374 (1977).
[47]C. G. Stevens and J. C. D. Brand, J. Chem. Phys. **58**, 3324 (1973).
[48]P. R. Bunker and S. R. Langhoff, J. Mol. Spectrosc. (to be published).
[49]P. R. Bunker, *Molecular Symmetry and Spectroscopy* (Academic, New York, 1979), p. 273.
[50]P. Phillips and E. R. Davidson, J. Chem. Phys. **76**, 516 (1982).
[51]C. E. Barnes, J. M. Brown, A. Carrington, J. Pinkstone, T. J. Sears, and P. J. Thistlethwaite, J. Mol. Spectrosc. **72**, 86 (1978).
[52]H. Petek, D. J. Nesbitt, and C. B. Moore, Paper TB-12, 38th Symposium on Molecular Spectroscopy, Columbus, Ohio, 1983; (private communication). These authors have observed part of the visible $\tilde{b}^1B_1$–$\tilde{a}^1A_1$ spectrum of CH_2 using magnetic rotation spectroscopy. Near the expected positions of a number of transitions involving the $\tilde{a}^1A_1(000)7_{16}$ level, they observe a pair of strongly magnetic lines with a spacing that is entirely consistent with our analysis (our calculated perturbed splitting between $\tilde{a}$ 7_{16} and the $J=7$ component of $\tilde{X}(030)6_{15}$ is 6.421 cm^{-1} from Table II). This observation provides further confirmation for the analysis presented in this paper, and also indicates that some of the assignments involving $\tilde{a}$ 7_{16} in Ref. 3 are incorrect. The same authors have also recently detected the ν_1 and ν_3 fundamental stretching bands within the $\tilde{a}^1A_1$ state of CH_2.
[53]G. Duxbury, J. Mol. Spectrosc. **25**, 1 (1968).